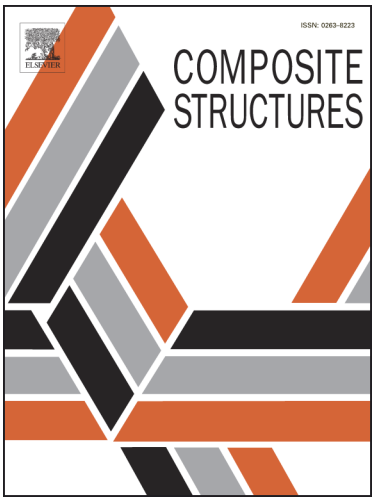

Performance of Precast Segmental Concrete Beams Posttensioned with Carbon Fiber-Reinforced Polymer (CFRP) Tendons

Tan D. Le, Thong M. Pham, Hong Hao, Cheng Yuan

PII: S0263-8223(18)31238-8
DOI: https://doi.org/10.1016/j.compstruct.2018.10.015
Reference: COST 10265

To appear in: *Composite Structures*

Received Date: 3 April 2018
Revised Date: 3 September 2018
Accepted Date: 4 October 2018

Please cite this article as: Le, T.D., Pham, T.M., Hao, H., Yuan, C., Performance of Precast Segmental Concrete Beams Posttensioned with Carbon Fiber-Reinforced Polymer (CFRP) Tendons, *Composite Structures* (2018), doi: https://doi.org/10.1016/j.compstruct.2018.10.015

Performance of Precast Segmental Concrete Beams Posttensioned with Carbon Fiber-Reinforced Polymer (CFRP) Tendons

Tan D. Le[1], Thong M. Pham[2], Hong Hao[3], and Cheng Yuan[4]

Abstract

Precast segmental prestressed concrete beams (PSBs) have been widely used in many elevated highway bridge projects around the world. Steel tendons at joint locations, however, are vulnerable to corrosion damages, which cause deteriorations and in extreme cases lead to the collapse of the whole structures. This study experimentally investigates the use of carbon fibre-reinforced polymer (CFRP) tendons as an alternative solution for the PSBs to tackle the corrosion issue. Four large-scale segmental T-shaped concrete beams with internal bonded or unbonded tendons and dry or epoxied joints were built and tested under four-point loading. The test results indicated that CFRP tendons showed satisfactory performances therefore could replace steel tendons for the use in PSBs. All the tested beams exhibited excellent load-carrying capacity and ductility. Tendon bonding condition greatly affected the flexural performance of the segmental beams. Joint type had only a slight effect on the load-carrying capacity and ductility of the beams, but significantly affected the beams' initial stiffness. Unbonded tendons experienced an evident reduction in the tendon strength at the ultimate stage as a consequence of the loading type, harping effect and joint opening. Both AASTHO-

[1]PhD Scholar, Center for Infrastructural Monitoring and Protection, School of Civil and Mechanical Engineering, Curtin University, Kent Street, Bentley, WA 6102, Australia. Email: tan.le1@postgrad.curtin.edu.au

[2]Research Fellow, Center for Infrastructural Monitoring and Protection, School of Civil and Mechanical Engineering, Curtin University, Kent Street, Bentley, WA 6102, Australia, (corresponding author). Email: thong.pham@curtin.edu.au

[3]John Curtin Distinguished Professor, Center for Infrastructural Monitoring and Protection, School of Civil and Mechanical Engineering, Curtin University, Kent Street, Bentley, WA 6102, Australia, and School of Civil Engineering, Guangzhou University, Guangzhou 510006, China, (corresponding author). Email: hong.hao@curtin.edu.au

[4] PhD Scholar, Center for Infrastructural Monitoring and Protection, School of Civil and Mechanical Engineering, Curtin University, Kent Street, Bentley, WA 6102, Australia. Email: cheng.yuan@postgrad.curtin.edu.au.

1999 and ACI 440.4R-04 predicted well the tendon stress, thus the load-carrying capacity of the beams with bonded tendons, however, the accuracy significantly reduced for the cases with unbonded tendons. Similarly, the codes did not well estimate the deformation capacity of the prestressed beams with unbonded tendons. An empirical formula is proposed to predict the deflections of beams with unbonded tendons, which yields very close predictions to the experimental results.

Keywords: Precast segmental structures; carbon fibre-reinforced polymer tendons; internally prestressed; bonding type; beam deformation.

1 Introduction

Precast segmental prestressed concrete beams (PSBs) have been widely used in many bridges around the world, especially in the United States, France, Spain and China over the past four decades. Time-saving and economic benefits are among the advantages that made the PSBs very well suited to the construction of the medium to moderate long-span bridges [1]. To date, steel tendons are used as the only prestressing material to join individual segments to form completed bridge spans. The tendons have been designed using internal tendons, external tendons or a combination of internal and external tendons. Corrosion problems of the steel tendons at segment joints, however, are a great concern of the application of PSBs, particularly in the places with highly aggressive environmental conditions. Inappropriate design choices and poor quality construction of the corrosion protection systems are the main factors that have been contributing to the corrosion-induced damages, which greatly increase and lifetime maintenance costs of such bridges. In extreme cases, the whole structure might even completely collapse as reported in previous studies [2-4].

Fiber-reinforced polymer (FRP) tendons are corrosion free and possess a high tensile strength that even exceeds steel tendons. Furthermore, they are lighter than steel, which allow easier handling and reduce dead load of the structure. As such, FRP tendons are likely to be a potential alternative to steel tendons for the precast segmental concrete beams to dealing with the corrosion issues. In the literature, the use of FRP tendons has only been applied to monolithic concrete beams while their application on PSBs has not been reported yet. It is noted that unlike steel tendons, FRP tendons show linear stress-strain relationship up to failure, lower elastic modulus and are weak in shear. These properties can possibly lead to higher deflections of the structure and premature failure of the tendons at the segment joints due to the stress concentration. It is therefore important to investigate the behavior of PSBs prestressed with FRP tendons before its possible practical applications. This study performs experimental tests to investigate the structural performance and ductility of segmental

concrete beams strengthened with FRP for possible use in PSBs.

2 Literature reviews

A large number of studies has been performed over the last four decades to investigate the structural behavior of precast segmental structures. An extensive literature review on segmental concrete beams prestressed with steel tendons either internal bonded/unbonded or external unbonded can be found elsewhere [5-7]. Key findings can be summarized as follows. Up to date, steel tendons have been the only prestressing solution to connect individual beam segments, forming the final bridge spans. Internal bonded tendons and epoxied joints are normally used in the first PSBs generations. This type of tendon is shown to be the most effective prestressing method for PSBs as it better mobilizes tendon strength at the ultimate, thus increases the beam's strength capacity, better maintains tendon eccentricity and allows the beam to achieve greater ductility under loads. However, it is difficult to monitor and check the bond quality between the tendon and concrete during grouting and during service life, and almost impossible to replace the tendon in the case of corrosion or other types of damage and deterioration.

External unbonded steel tendons are then introduced to the next PSBs generations. The use of external tendons along with dry joints is considered the fastest way to construct the precast segmental beams. Corrosion problems are also greatly improved since external tendons are easier to handle, monitor and replace when necessary. Detailed discussions of advantages and disadvantages of the external unbonded tendons are given in previous studies [1, 8, 9]. However, a reduction in the capacity of the externally unbonded prestressed PSBs in both strength and ductility is evident. Breakdown of deviators or anchorage systems can cause catastrophic failure due to the sudden loss of the prestressing force, which is a concern of using the external unbonded system.

PSBs with a mixture of external and internal tendons were recently studied by researchers.

This combination takes advantage of both types of tendons, i.e. the internal tendons can improve the ductility of the beam, and the external tendons are convenient for maintenance. Yuan et al. [6] and Yuan et al. [10] conducted a series of tests to investigate the behavior of PSBs with hybrid tendons and epoxied joints. The specimens were designed with different ratios of the external and internal tendons and were then tested under monotonic vertical loading. The test results indicated that the ratio of the hybrid tendons significantly affected the strength capacity and ductility of the segmental beams. The more internal bonded tendons were used, the higher were the load-carrying capacity and better ductility. As such, the ratio of internal to external tendons not less than 1:1 was recommended. Jiang et al. [5] investigated the flexural behavior of PSBs with hybrid tendons and dry joints. The beams had T-shape cross-section and were post-tensioned with either external tendons or hybrid tendons, which were all unbonded to the concrete. It was found that the use of hybrid tendons enhanced the flexural behavior of the segmental beams and increased both the ultimate bending capacity and ductility compared to beams with solely external tendons. Furthermore, there was no significant difference between the stress increments of the internal and external tendons as a result of the bond absence between the internal tendons and surrounding concrete.

Joints between segments are the most critical part of PSBs as they ensure the shear transfer and integrity of the whole structure. The joints can be epoxied or dry, flat or keyed, and single or multiple shear keys made of plain concrete or reinforced concrete. Extensive studies on the behavior of joints under direct shear are available in the literature, which was reviewed elsewhere [11, 12]. Meanwhile, little research has been carried out on the behavior of joints under combined shear and bending [7]. For brevity, only some recent studies on the flexural behavior of PSBs that focus on the joint performance are reviewed here. Saibabu et al. [13] conducted an experimental program to evaluate the performance of dry and epoxied joints in precast segmental box girders under monotonic and cyclic loading. It was found that the applied load at the maximum and at the failure of the beams with dry joints were less than

those with the epoxied joints because of the high concentration of rotation and deflection at individual dry joints of the beams. Although the dry joints opened at a lower load compared to the epoxied joints, both the beams achieved almost the same deflection at failure. In addition, both joint types underwent significant repeated openings and closures during cyclic loading tests without failure. Li et al. [7] studied the behavior of joints when they were subjected to the combined shear and bending. Both dry and epoxied joints were used in the specimens. The authors concluded that when a precast segmental beam subjected to vertical loads located at the immediate vicinity of the joint, the failure of the beam was different from the traditional bending failures and shear failures, and the failure of epoxied joints was also different from that of dry joints. In the case of the epoxied joints, the failure cracks propagated vertically in the concrete adjacent to the segment interface but did not develop toward the loading point. In contrast, the failure of the dry joints occurred in the segment interface. Also, join position had a significant effect on the joint strength when the applied loads were in the immediate vicinity of the joints. When the joint was close to the midspan, the joint strength was reduced.

In the literature, the use of FRP tendons has only been applied to monolithic concrete beams. A lot of research work has been done to investigate the flexural behavior of the monolithic beams prestressed with FRP tendons. Extensive literature review on the matter can be found elsewhere [14, 15]. Here, only studies to address the differences in the structural behavior of a beam prestressed with FRP tendons and the one with steel tendons are briefly reviewed. For an FRP prestressed beam, when the tendon is internally bonded to the concrete, it shows different behavior to the steel prestressed beam after concrete cracking [16-18]. Both the beams exhibit a linear relationship between the applied load and midspan deflection in the first stage. However, after cracking the steel prestressed beam deforms nonlinearly up to the failure. Whereas, FRP prestressed beam continues to deform in an approximately linear manner with the applied load until failure.

In contrast, in the cases of unbonded tendons, both FRP and steel prestressed beams show similar behavior under the applied load up to the ultimate stage [19-21]. Pisani [20] conducted a numerical investigation on beams prestressed with FRP tendons. Prestressing types including bonded/unbonded internal, external, and the tendon types including steel and GFRP were studied. It was observed that the structural behavior of beams prestressed with unbonded FRP tendon was similar to beams with unbonded steel tendons. However, the low creep rupture limitation of the GFRP tendons, normally less than 30%f_u, greatly restricted its high efficiency in prestressing application. Similar behaviors were reported by Lou et al. [21] on beams internally prestressed with unbonded CFRP and steel tendons. The type of unbonded tendons had limited influence on the cracking mode, deformation capacity, stress increments in the unbonded tendon and in the non-prestressed steel, and had practically no influence on the development of moment redistribution. Tan and Tjandra [19] tested continuous beams and concluded that the use of external CFRP tendons did not lead to significant differences in terms of the ultimate load, tendon stress, and deflection as compared to beams with steel tendons.

When FRP tendons are deviated, stress concentration in the tendons due to harping effect is an issue that needs due care. This stress concentration phenomenon adversely prevents the increase in the tendon stress because FRP tendon is made of an anisotropic material, it has very low transverse strength as compared to its tensile strength. The deviator curvature, harping angle, and tendon size are observed to be the main factors impacting the stress increments in the tendon regarding the harping effect. Mutsuyoshi and Machida [22] found that CFRP tendons with 400 mm diameter steel deviators ruptured at 77% and 80% of their breaking load when deviated at angles of 7.1^o and 11.3^o, respectively. Grace and Abdel-Sayed [23] reported 19% and 34% reductions in breaking forces for carbon fiber composite cable (CFCC) tendons draped at 3^o angle and 5^o angles when using 50.8 mm diameter deviators, respectively. When 508 mm diameter deviators were used, those reductions were 12% and

26% at draping angles of 5^o and 10^o, respectively. Wang et al. [24] recommended the harping angle should be less than 3^o to avoid the strength reduction percentage exceeding 10%. Quayle [25] reported reductions ranging between 13% and 50% in the tensile strength of the CFRP tendons when the tendons were draped at 2^o to 15^o using deviators of the radius of 50 mm to 1000 mm, respectively.

Many efforts have been paid to overcome the corrosion problems of the steel tendons that, however, are still a great concern of PSBs. FRP tendons have been widely used for monolithic beams as a promising solution to replace steel tendons owning to its excellent properties such as high corrosion resistance, and high strength-to-weight ratio. The use of FRP tendons on precast segmental structures has not been reported yet. As such, the possible use of FRP tendons for post-tensioning PSBs is investigated in the present study.

3 Experimental program

Four large-scale precast segmental concrete T-shape beams were built and tested in the Civil Engineering Laboratory, Curtin University to investigate the flexural behavior of PSBs prestressed with CFRP tendons. Both internal bonded and unbonded CFRP tendons, together with two types of joints, i.e., dry and epoxied multiple shear-keyed joints were used in the beams. All the beams were then cyclically tested under four-point loading up to failure. Details of the specimen design and test set up are presented in the following sections.

3.1 Design of specimens

The beams were designed in accordance with the AASHTO [26] and ACI 440.4R [17]'s requirements. All the beams had T-shape cross-section of 400 mm height and 3.9 m overall length. Each beam consisted of four segments which were made of reinforced concrete ranging from 800 mm to 1150 mm length. The detailed dimensions of the tested beams are given in Fig. 1. These segments were joined together by two CFRP tendons for each beam using the common post-tensioning technique. Table 1 gives the detailed configuration of the

specimens, in which Beams C1 and C2 contained bonded tendons but different joint types, and Beams C3 and C4 had unbonded tendons and different joint types.

Previous studies showed that the shear stress distribution in the multiple shear-keyed joints, which are widely used in practice, is more uniform than in the single keyed joints [7, 27]. Therefore, multiple shear-keyed joints were adopted in this study. The keys had the same cross-section dimensions but different lengths on the flanges and on the webs of the specimens as shown in Fig. 2.

Each segment of a beam was reinforced with a minimum amount of non-prestressed reinforcement at the top and bottom of the segment. This minimum amount reinforcement was computed according to the requirement of ACI 318-14 [28], i.e. $A_{s,min} = 0.004A_{ct}$, where A_{ct} is the area of the cross-section part between the flexural tension face and the centroid of the gross section. Hence, two 12 mm diameter deformed bars were used for the bottom longitudinal reinforcements and 10 mm diameter deformed bars were used for the top layer. These steel bars were cut off leading to the discontinuity of the longitudinal steel reinforcement at the joint locations. 10 mm diameter deformed bars were also used for the transverse reinforcements which were placed at 100 mm spacing for the two middle segments and at 75 mm spacing for the two end segments to strengthen beams in shear (Fig. 1).

3.2 Materials

Pre-mixed concrete was used in the specimens and was supplied by a local supplier. The average compressive strength of concrete cylinders on the testing day was 44 MPa. Single strand CFRP tendons of 12.9 mm diameter were used in the specimens, which were supplied by Dextra Building Products CO., LTD [29]. Conventional steel bars of 12 mm and 10 mm diameters were used for longitudinal and transverse steel reinforcements, respectively, and the mechanical properties are given in Table 2.

3.3 Fabrication

Reinforcing steel cages of each segment were manufactured and placed in a timber formwork. Corrugated metal duct of 40 mm diameter was also mounted into the steel cages to create holes for installing tendons later. Separation plates of T-shape timber were positioned in the formwork at designed distances to separate segments during pouring concrete. Foam moulds of shear-keyed shapes were attached to the separation plates to form the shear keys as shown in Fig. 3.

Match-casting method was employed to cast the segments, in which the first and third segments were cast in the first concrete batch, and then they were used as a formwork to create the second and fourth segments in the second batch. Thereby, the male and female keys between two adjacent segments were assured to perfectly fit. Concrete cylinders of 100 mm diameter and 200 mm height were also made from the premixed concrete to ascertain its properties.

After casting, all the segments were left to cure in a moist condition, in which wet hessian rags were placed on top of the segments and were watered twice a day to keep them moist. The formwork was removed after 7 days of casting, then the segments were left for continuous curing at least 28 days before post-tensioning and testing.

3.4 Epoxy and grouting

For the beams with epoxied joints, the key surfaces were thoroughly cleaned using a steel brush and an air gun to make sure the surfaces in a good condition and free from dust (Fig. 4a). The concrete surfaces were then thoroughly watered and left to dry for at least 2 hours before applying the adhesive. A thin layer of Sikadur-30 [30] was applied to the joint surfaces of the segments using a painting brush and a trowel. After post-tensioning, the epoxied beam was left for curing of the adhesive for 3 days (Fig. 4b).

For the beams with bonded tendons, grouting was done after the completion of post-

tensioning. The metal duct was carefully cleaned using a high-pressure air gun to ensure the ducts free of dirt and debris before placing and stressing the tendons. SikaGrout-300PT was used in the specimens, which was mixed by a grout mixer [31]. The grout was then injected into the ducts via the PVC pipes at one end using a manual grout pump until it came out from the other end. The beams were left for 7 days for curing of the grout (Fig. 4c).

3.5 Post-tensioning

A typical set up of post-tensioning is given in Fig. 5. Steel couplers were used to connect the CFRP tendon to a steel tendon of 1.5 m length. Thus, the stressing procedure for the CFRP tendons was done in the same way to the steel tendons. The stressing force was generated by a hydraulic jack placing on a jacking chair. Two sets of anchors including wedges and barrels were used in the stressing end, in which one was placed after the hydraulic jack so-called post-tensioning anchor No. 2 and one placed before the jack so-called working anchor No. 1. Tightening system including hollow bolts and nuts was mounted inside the jacking chair just before the working anchor No.1 for tightening and releasing the force after testing. Load cells were used to monitor the tensioning force produced by the jack and to measure the force in the tendons after transfer.

The stressing procedure was done as follows. In the first step, the tendons were stressed an initial force of approximately 10% of the total stressing force to close the gaps between segments and to remove the slack. The total stressing force was computed from the control stress in the tendons, which were taken as 0.4 f_{pu} for CFRP tendons [17]. Each tendon was then tensioned in three load levels at 20%, 60% and 100% of the total stressing force until completion. Load cells and strain gauges attached to the tendons were used to monitor and measure the stresses in the tendons during the post-tensioning process. The effective tendon stresses and the corresponding force in the tendons immediately following transfer are given in Table 1.

3.6 Instrumentation and loading

Fig. 6 shows a typical test set up. The applied load was generated by two vertical hydraulic jacks, which were placed equally at one-third span. Two horizontal I-steel spreading beams were used to transfer the vertical loads from the jacks uniformly across the beam sections. Load cells were used to monitor the applied load generated by the hydraulic jacks. Linear variable differential transformers (LVDTs) were used to measure the vertical displacement and opening of joints. Strain and posttensioning force in the conventional steel bars and the CFRP tendons were measured by strain gauges and load cells attached at the end of the beams. All the beams were cyclically tested under four-point loading test up to failure, in which each load level increased by 20 kN and two cycles were performed at each load level. In one cycle, the applied load increased gradually to the desired value then reduced to about 5 kN before starting next cycles, excluding the first load cycle when the applied load started from 0. All the tests were conducted under the load control at a rate of approximately 3 to 5 kN/min.

4 Experimental results and discussions

4.1 Summary of tested results

The test results for all the specimens are given in Table 3, in which P_{cr}, $\delta_{mid,cr}$, $\Delta_{J,cr}$ and P_u, $\delta_{mid,u}$ and $\Delta_{J,u}$ are the applied load, midspan deflection, and opening of the middle joint of the specimens at cracking and at the ultimate stage, respectively. It is noted that the applied load, corresponding midspan deflection and joint opening of Beams C1 and C3 at the cracking are taken as yielding values as defined by Park [32] and is illustrated in Fig. 7.

Photos of the specimens' failures are presented in Fig. 8 (a-d), which clearly show different failure modes of the tested beams. Beams C1 and C2 with bonded tendons failed by rupture of CFRP tendons without any concrete spalling on the top while Beams C3 and C4 failed by concrete spalling on the compressive side and CFRP tendons rupturing at the bottom. The

concrete crushing or the rupture of tendons occurred at the middle joint at the midspan for all the specimens.

The load-deflection curves of the specimens and their corresponding envelops are plotted in Fig. 9 and Fig. 10. It is observed that the beams with bonded tendons showed much higher strengths but lower ductility compared to the beams with unbonded tendons. The ultimate strengths of Beams C1 and C2 were an average of 167 kN which was 41.5% higher than those of Beams C3 and C4 at an average of 118 kN. In contrast, Beams C1 and C2 only experienced 47.2 mm deflection on average at the ultimate stage which was about half of the maximum deflections observed in Beams C3 and C4, which was 97.9 mm on average.

It is worth noting that even though the ultimate deflections of Beams C1 and C2 were much smaller than those of Beams C3 and C4, these values well satisfied the maximum allowable midspan deflection specified by AASTHO LRFD [37]. AASTHO LRFD [38] limits the maximum deflection to 1/800 of the beam's span length while Beams C1 /C3 and C2/C4 in this study underwent deflections of approximately 1/75 and 1/37 of the beam's span lengths at the ultimate stage, respectively. In addition, the experimental results from the previous studies [33, 34] on both segmental beams with unbonded steel tendons and CFRP tendons showed that the beams with unbonded CFRP tendons even achieved larger deflections at the ultimate stage compared to the beam with unbonded steel tendons. The ultimate deflection of the beam with unbonded steel tendons was equal to approximately 1/40 (89.4 mm) of the beam's span length. Further analyses and discussions regarding the flexural behavior of PSBs with unbonded steel and CFRP tendons can be found in the previous studies [33, 34]. CFRP tendons could, therefore, well replace the steel tendons for the use in the precast segmental concrete beams to overcome the possible corrosion-induced damage frequently observed in this type of structures.

Two stages can be identified for the load-deflection curve of each specimen with one inflection point representing the cracking of concrete at the bottom fiber for the beams C2 and

C4 with epoxied joints or the opening of the middle joint for the beams C1 and C3 with dry joints, which are similar to the behavior observed on segmental beams with external steel tendons reported in the previous studies [7, 13]. This observation is different from the cases of monolithic beams with unbonded tendons, where the load-deflection curves exhibited almost three distinct stages due to the presence of reinforcing steel, which exhibits a further inflection point when the reinforcing steel yields [24, 35].

4.2 Effect of bonding condition on structural behavior

Bonding condition between the tendon and concrete strongly affected the flexural behavior of the beams. The use of bonded tendons significantly increased the strength of the precast segmental beams as observed in Beams C1 and C2 while the use of unbonded tendons greatly improved the ductility of Beams C3 and C4. This can be explained by a well-known fact that the change in the tendon strain of a bonded tendon is sectional dependent while that in an unbonded tendon is member dependent [36, 37]. As a result, at the same level of concrete strain in the compressive top fiber of the section, the beam with bonded tendons more effectively mobilizes the strain in the tendon, and hence the tendon strength as observed later in Fig. 16, leading to the higher load carrying capacity. Meanwhile, the strain change in the unbonded tendons is relatively uniformly distributed to the whole length of the tendons, rather than concentrated at a single section, which allows the beam to achieve larger deflection. As such, the selection of bonded or unbonded tendons depends on the actual design requirement.

Bonding condition of the tendons also affected the stiffness of the beams. By comparing the load-deflection curves of Beams C1 and C3 (Fig. 10), it can be observed that Beam C1 exhibited higher stiffness than Beam C3 and the difference in the beams' stiffness became considerable when the applied load reached about 54 kN as the middle joint started to open highly. In the meantime, Beam C3 substantially lost its stiffness while Beam C1 still showed high stiffness. This is because the use of the bonded tendons in Beam C1 helped restrain the

detachment of the two adjacent segments preventing the reduction in the beam's section height.

In contrast, the bonding type had no effect on the initial stiffness of the epoxied joints beams. This is reasonable since both the beams with epoxied joints behaved like monolithic beams before cracking, thus no changes in the section geometry leading to the same initial stiffness as observed in Fig. 10. After cracking, Beam C2 still showed high stiffness while Beam C4 substantially lost its stiffness, which again clearly demonstrates the effectiveness of the bonded tendons regarding the strength enhancement of the beams.

The failure modes of the beams were also affected by the bonding condition of the tendons. All the beams in this study were under-reinforced, consequently, the failure mode would theoretically be controlled by tension since $c/d < 0.42$ by AASHTO LRFD [38] as observed in Beams C1 and C2. However, the use of unbonded tendons shifted the failure mode of Beams C3 and C4 from tension controlled to compression controlled as they showed severe concrete crushing on the top fiber before the rupture of the tendons at the ultimate stage. This phenomenon is attributed to the member dependence of the unbonded tendons as discussed above. The failure in Beams C3 and C4 occurred gradually and less explosive than that in the Beams C1 and C2 with bonded tendons. Effects of the tendon bonding condition on the beam's crack pattern, joint opening, and the strains in the tendon and steel reinforcements will be discussed in subsequent sections.

4.3 Effect of joint types on structural behavior

By comparing the load-deflection curves of Beams C1 versus C2 and Beams C3 versus C4, it can be observed that regardless of the tendon bonding condition, the type of joints had only a slight effect on the load-carrying capacity and ductility of the beams, but significantly affect the beams' initial stiffness. Both Beams C1 and C2 had similar strength and deflection at the ultimate stage as mentioned previously, and that was also true for the cases of Beams C3 and

C4, although both Beams C2 and C4 with epoxied joints showed a bit higher ultimate strength than those of their counterparts with dry joints, Beams C1 and C3, by 3.1% and 8.8%, respectively.

Both Beams C2 and C4 had an initial stiffness of approximately 22.5 kN/mm, which were about 2.8 and 3.5 times those of the counterparts with dry joints C1 and C3, respectively. This means that at the same load levels in the elastic region, a beam with dry joints and bonded tendons will experience deformations 2.8 times that of the equivalent beam with epoxied joints and that deformation is even higher at 3.5 times when the unbonded tendons were used, which once again demonstrates the effect of bonding condition of the tendons on the structural behavior of the beams. This observation needs to be taken into account in the design of a bridge structure since main components of the structure are designed to be working in the elastic limit, especially in the service limit stage when the elastic deformations of the structure are checked.

4.4 Crack patterns

Cracking patterns of the tested beams are greatly affected by the bonding condition of the tendons. When bonded tendons were used, the beams could develop both flexural and shear cracks regardless of the joint type used as clearly observed in Fig. 8 (a,b). Both Beams C1 and C2 exhibited similar crack patterns regarding the crack width, crack length and uniformly distributed along the beams' axis, which was similar to the crack pattern of a traditional monolithic prestressed concrete (PC) beam. The crack propagation of Beam C2 was noted as follows. When the applied load was about 54 kN, one vertical crack appeared at the middle joint at the midspan with cracking sounds that vertically cut off all the shear-keyed bases of the joint as seen in Fig. 8b. The crack was at a certain height of the section at the beginning and then gradually developed vertically to the top under the increase in the applied load. Soon after, vertical cracks were also formed at Joints J1 and J3 (refers to Fig. 8 for joints' locations)

that also cut off all the shear-keyed bases of the joints. When the applied load reached about 85 kN to 90 kN, flexural and shear cracks were observed at bottom of the beam. These cracks were symmetrically developed on each side of the beam until the beam failed by the rupture of the tendons, which occurred at the middle joint at the midspan. The crack propagation of Beam C1 was very similar to that of Beam C2. The only difference was that the vertical cracks at the joints J1 to J3 already existed since dry joints were used. It is worth noting that, although the crack pattern of Beams C1 and C2 was very similar to that of a PC beam, the crack propagation was different. In the segmental beams, flexural cracks occurred at joint locations first and then the flexural cracks within the segments appeared due to the contribution of reinforcing steel of the segments, which did not exist at joint locations. Meanwhile, in a PC beam, the flexural cracks normally develop at the midspan and then spreads gradually to the ends under the increases of the applied load. The crack propagation of a segmental beam, however, should be analyzed together with the effects of the number of segment and the segment length in practical situations.

Conversely, due to the lack of restriction of the unbonded tendons, no cracks were observed in the cases of Beams C3 and C4. Although Beam C4 developed a vertical crack at the middle joint J2, the crack was, in fact, the opening of the epoxied joint when the applied load exceeded the cracking load. Therefore, the contribution of the normal reinforcing steel to the flexural capacity of the segmental beams should be considered depending on the bonding condition of the prestressing tendons.

4.5 Joint openings

The openings of all the joints along the beams' axis at the ultimate stage are plotted in Fig. 11. It is observed that the opening of the joints was greatly affected by the bonding conditions of the tendons regardless of the joint type. All the joints of the beams with bonded tendons opened at the ultimate load and the opening of the joints proportionally distributed along the

beams' axis. In contrast, in the cases of the beams with unbonded tendons, only the middle joint opened while the others almost remained closed. In the cases the tendons were bonded to the concrete within the segments, the separation of the two adjacent segments, thus the opening of the joints was equal to the extension of the tendon between the joints. As such, the joint opening distribution in Beams C1 and C2 would be comparable to the tendon strain distribution along the beams' axis, as observed in Fig. 11. The lack of bonding between the concrete and the tendons in Beams C3 and C4 caused large opening of the middle joint under the applied load. The opening of the middle joint might be the factor to restrain the other joints. This observation supports the assumption that the beam with unbonded tendons develops one major crack at the midspan at the ultimate stage, which is used to calculate the plastic hinge length, thus the stress in the unbonded tendons in several models [39-41].

The opening of the middle joint with respect to the applied load for the specimens are given in Fig. 12. It is observed that the middle joint in Beams C1 and C3 started to open soon after the load was applied since dry joints were used in these beams. The gradual opening of the joint leads to the smoother change in the beam's stiffness compared to the corresponding beams with epoxied joints as observed in Fig. 10. Meanwhile, the middle joints in Beams C2 and C4 still remained closed until cracking load was reached. At the ultimate load, the middle joint of Beams C1 and C2 exhibited almost equal openings at 4.73 mm and 4.30 mm, which were much smaller than those of Beams C3 and C4 at 27.7 mm and 30.02 mm, respectively, which again demonstrates the effect of bonding the tendon in construction.

The opening of the middle joint with respect to the midspan deflection is also plotted in Fig. 13. It can be seen clearly that the opening of the joint showed an approximately linear relation with the midspan deflection of the beam under the applied loads. In the cases of the epoxied joints beams, it can be stated that the width of the vertical crack developed linearly with the midspan deflection of the beam under the loads. However, it is worth noting that this linear relationship is only valid when the applied load went beyond the cracking load. Before that

load value, the epoxied joints still remained closed.

4.6 Load-strain relationships

Fig. 14 shows the load-strain relationships of the conventional longitudinal steel rebars and CFRP tendons in Beams C3 and C4. It is observed that after the opening of the joint, the strain in the CFRP tendons in the two beams started to increase significantly that were approximately linear to the applied load, while the strain in the steel rebars almost maintained constant at a very small value of around 100 μm/mm. This result indicates that the tension force was mainly contributed by the CFRP tendons and almost no any contribution of the steel rebars because they are discontinuous at the joints. The strain in the steel rebars also explained why no flexural crack was observed at the bottom of the segments in Beams C3 and C4 as discussed above. The ultimate strain of the CFRP tendons in Beams C3 and C4 were 1.22% and 1.16%, which were only equal to 72% and 69% of the nominal tensile strain of the tendon.

In contrast, the steel rebars in the beams with the bonded tendons yielded as shown in Fig. 15, leading to the flexural cracks observed at the segment bottom of Beams C1 and C2 as shown in Fig. 8 (a,b). CFRP tendons showed a greater strain increments compared to the steel rebars since only CFRP tendons contributed to the tension force at the joint locations and the strain measurement of the steel rebars was taken at the middle of the segment, which was not at the middle joint at the midspan as in the case of CFRP tendons. Similar to the cases of Beams C3 and C4, Beams C1 and C2 also exhibited an approximately linear relationship between the tendon strain, thus the tendon stress and the applied load after the opening of the joints. The tendon strains at the ultimate stage reached about 93% of the nominal tensile strain on average in the cases of Beams C1 and C2 with bonded tendons.

4.7 Stress increment in the CFRP tendons

Fig. 16 shows the tendon stress increment with respect to the applied load for the specimens.

It is observed from the figure that the tendon stress in all the beams started to increase from the beginning of the test. However, the increment rate in the tendon stress just prior to the cracking of concrete or opening of the joint (before the inflection point) was very small showing approximately 6% to 8%. The tendon stress increment was due to the beam's deflection under the applied load. All the beams exhibited an approximate bilinear relationship between the applied load and tendon stress increment.

By comparing the stress increment curves of Beams C1 versus C2 and Beams C3 versus C4, it is observed that the curves of the two beams with bonded tendons or the two with unbonded tendons exhibited almost similar trends (Fig. 16). This indicated that the type of joints had only a slight effect on the increase in the tendon stress. The stress increment in the beams with bonded tendons was approximately 54% of the nominal tensile strength of the CFRP tendons, f_{pu}, while that was of 40% f_{pu} in the cases of the beams with unbonded tendons.

The relationships between the stress increment and the midspan deflection for the beams are also plotted in Fig. 17. It is observed that the change in the tendon stress exhibited an approximately linear manner with the midspan deflection for all the beams regardless of the tendon bonding condition and the joint type. This observation is similar to the previous studies conducted on monolithic beams prestressed with unbonded tendons [24, 35, 42]. As such, it supports the calculation of the stress increment in the CFRP prestressed PSB beams based on the midspan deflection as in the cases of monolithic beams [43, 44]. Since the opening of the joints represents the elongation of the tendon as a whole, approximately linear relationships were also observed between the stress increment and the joint opening in all the specimens as shown in Fig. 18.

5 Theoretical considerations

5.1 Beams' strength

The strength capacity of the beams were calculated in accordance with the design procedure

recommend by AASHTO [26] and ACI 440.4R [17]. However, it is noted that none of these equations addresses precast segmental beams with CFRP tendons. The design equations presented in AASHTO [26] are used for segmental beams prestressed with steel tendons while those in ACI 440.4R [17] are for monolithic beams with FRP tendons. AASHTO [26] adopted the following expressions to compute the stress in the tendons. For bonded tendons AASHTO LRFD [38]:

$$f_{ps} = f_{pu}\left(1 - k\frac{c}{d_{ps}}\right) \tag{1}$$

in which $k = 2\left(1.04 - f_{py} / f_{pu}\right)$; f_{pu} is the nominal tensile strength of the tendon; f_{py} is the yield strength which is taken as f_{pu} since CFRP is a linear elastic material; c is the neutral axis depth at the ultimate stage, d_{ps} is the distance from the extreme compression fiber to the centroid of the tendons. For unbonded tendons:

$$f_{ps} = f_{pe} + 6200\left(\frac{d_{ps} - c}{l_e}\right), MPa \tag{2}$$

where f_{pe} is the effective tensile stress of the tendons, $l_e = L/(1+[N/2])$, in which L is the length of the tendon between anchorages, and N is the number of support hinges required to form a mechanism crossed by the tendon.

ACI 440.4R [17] recommended Eq. (3) to predict the stress in the unbonded FRP tendons at the ultimate. The nominal tensile strength f_{pu} is used in the case of beams with bonded tendons.

$$f_{ps} = f_{pe} + \Omega_u E_{ps}\varepsilon_{cu}\left(\frac{d_{ps}}{c_u} - 1\right) \tag{3}$$

where E_{ps} is the tendon modulus of elasticity; ε_{cu} is the ultimate concrete compression strain which was taken as 0.003; and Ω_u is a strain reduction coefficient which is defined as $\Omega_u = 1.5/(L_b/d_{ps})$ for one-point midspan loading and $\Omega_u = 3/(L_b/d_{ps})$ for uniform or third-point

loading, where L_b is the span length.

Strain compatibility analysis was then used for computating the flexural resistance of the specimens. The computed results are given in Table 4 and Table 5. It is seen from the tables that both the codes predicted well the stress and corresponding flexural capacity of the beams, although the experimental stress values were a bit smaller than those of theoretical calculations. Both the codes showed only 1% to 5% differences in the prediction of the load bearing capacity of the bonded tendons beams.

In the cases of beams with unbonded tendons, the accuracy of the code equations significantly reduced. AASTHO specification [26] underestimated the stress in the unbonded tendons, in which the predicted stress values were of only 76% and 71% of the experimental results for the tendons in Beams C3 and C4, respectively. As a result, the load bearing capacities of the two beams predicted by this code were also lesser than the experimental results, which were of approximately 82% and 67%, respectively. In contrast, ACI 440.4R [17] highly overestimated the stress in the tendons, thus the load carrying capacity of the two beams at the ultimate stage. The tendon stresses predicted by this code was approximately 20% higher than the experimental values. The reason for this substantial difference may lie on the length-to-beam's depth ratio *L/d*. ACI 440.4R [17] limits the application of Eq. 3 for beams prestressed with CFRP tendons having the unbonded length greater than 15 times the depth of the beam. In this study, the unbonded length tendon-to-the beam's depth was equal to 9.

5.2 Deflection calculation for beams with bonded tendons

The short-term deflection of the tested beams with bonded tendons was calculated using two methods, bilinear approach and effective moment of inertia, which were recommended by PCI [45], AASHTO LRFD [38] and ACI 440.4R [17]. In the bilinear approach, the total deflection of the beam, Δ, is the sum of deflections Δ_1 due to the load leading to cracking based on the gross moment of inertia of the concrete section, I_g, and Δ_2 due to the increment

of load from cracking to the ultimate using the moment of inertia of a cracked section, I_{cr}. PCI [45] suggested the following expression to calculate I_{cr} :

$$I_{cr} = nA_{ps}d_{ps}^2\left(1-1.6\sqrt{n\rho_{ps}}\right) \tag{4}$$

where n is the modulus ratio between the prestressing tendon and concrete, A_{ps} is the area of the prestressing tendon, and ρ_{ps} is the reinforcement ratio.

In the second method, an effective moment of inertia, I_e, is firstly determined and the deflection is then calculated for the total load by substituting I_e for I_g. The effective moment of inertia is recommended by AASTHO LRFD [38] as follows:

$$I_e = \left(\frac{M_{cr}}{M_a}\right)^3 I_g + \left(1-\left(\frac{M_{cr}}{M_a}\right)^3\right) I_{cr} \le I_g \tag{5}$$

in which M_{cr} is the cracking moment and M_a is the is the maximum moment in the member at which the deflection is being computed. ACI 440.4R [17] adopted the following equation to calculate I_e, which accounts for the reduced tension stiffening in FRP-reinforced members:

$$I_e = \left(\frac{M_{cr}}{M_a}\right)^3 \beta_d I_g + \left(1-\left(\frac{M_{cr}}{M_a}\right)^3\right) I_{cr} \le I_g \tag{6}$$

in which β_d is the softening factor given by:

$$\beta_d = 0.5\left[\frac{E_p}{E_s}+1\right] \tag{7}$$

and

$$I_{cr} = \frac{b(kd)^3}{3} + nA_{ps}(d-kd)^2 \tag{8}$$

where E_p is the modulus of elasticity of FRP tendon, E_s is the modulus of elasticity of steel, b is the width of the section, d is the distance from the extreme compression fibre to the

centroid of prestressing steel, and *k* is ratio of the neutral axis depth to the FRP tendon depth.

5.3 Deflection calculation of beams with unbonded tendons: proposed changes

The deflection calculation of a beam with unbonded tendons is more complex than for bonded tendons, since the strain compatibility at critical sections is not maintained. Therefore, the strain reduction factor, Ω, developed by Naaman and Alkhairi [37] is employed in this study to convert the strain behaviour of a unbonded tendon into an equivalent behaviour of a bonded tendon, then bilinear approach suggested by PCI [45] as mentioned previously is used to calculate the total deflection of the beams. The closed-form equation for computation of deflections can be expressed as follows Branson [46]:

$$\Delta = KML^2 / E_c I \tag{9}$$

then,

$$\Delta = \Delta_1 + \Delta_2 \tag{10}$$

where,

$$\Delta_1 = KML^2 / E_c I_1 \tag{11}$$

$$\Delta_2 = KML^2 / E_c I_2 \tag{12}$$

in which, K is a deflection coefficient that depends on the loading type and support conditions, for the two third-point loading test and two harped-point tendon profile for the beams in this study, $K = 23/216$ [47]; M is the applied moment; L is the span length; E_c is the concrete modulus of elasticity; and I_1 and I_2 are the moment of inertia of the section corresponding to loading stages.

The methods presented in the codes for estimating the displacement of epoxied joint beams do not predict well for dry joint beams because they do not consider the reduction of the beam stiffness in the dry joint beams. Therefore, the proposed method in this study takes the reduction in the beam stiffness of the dry joint beam into consideration. In the first stage of loading, when the beam is still in the elastic uncracked state, I_1 is proposed to be taken as

follows:

$$I_1 = \begin{cases} I_g & \text{for beams with epoxied joints;} \\ \left(f_{pe} / f_{pu} \right) I_g & \text{for beams with dry joints, bonded tendons;} \\ \left(f_{pe} / f_{pu} \right) \Omega I_g & \text{for beams with dry joints, unbonded tendons.} \end{cases} \quad (13)$$

in which $\left(f_{pe} / f_{pu} \right)$ represents the reduction in the section stiffness when dry joints are used resulting in no contribution of concrete in tension, $\left(f_{pe} / f_{pu} \right) \Omega$ accounts for the effect of strain reduction in the beams with unbonded tendons. The values of Ω in the elastic uncracked state for most common loading conditions and tendon profiles are calculated and given in Table 1 of Naaman and Alkhairi [37], $\Omega = \frac{44}{81} + \frac{10}{81} \frac{e_s}{e_m} = 0.61$ is adopted for the beams in this study, where e_s and e_m are the tendon eccentricities at the supports and at the midspan.

After cracking, I_2 is taken as I_{cr}, which is calculated herein based on the cracked section analysis (Fig. 19). From the cracked section analysis of a reinforced concrete beam, one important relation between the steel stress, f_s, and the concrete stress at the location of steel, f_{ct}, is found as $f_s / f_{ct} = n$, where n is the modulus ratio. Applying this observation for the prestressed concrete, neglecting the depression strain of concrete due to prestressing since it is very small [17], we have the following relations:

For a bonded tendon:

$$n = \frac{E_{ps}}{E_c} = \frac{E_{ps} \varepsilon_{ct}}{E_c \varepsilon_{ct}} = \frac{E_{ps} \Delta \varepsilon_{ps}^{bonded}}{E_c \varepsilon_{ct}} = \frac{\Delta f_{ps}^{bonded}}{f_{ct}} \quad (14)$$

For an unbonded tendon, n_{unb} is defined as follows:

$$n_{unb} = \frac{\Delta f_{ps}^{unbonded}}{f_{ct}} = \frac{\Omega_u \Delta f_{ps}^{bonded}}{f_{ct}} = \Omega_u n = \Omega_u \frac{E_{ps}}{E_c} \quad (15)$$

Then, to find the modulus of inertia of the cracked section, it is assumed that the amount of prestressing tendons is replaced by an equivalent amount of concrete, which is proposed to be equal to $\Omega_u n A_{ps}$. Taking the first moment of the cracked section area with respect to the reference axis, the neutral axis c can be determined from the following quadratic equation for T-sections:

$$\frac{1}{2}b_w c^2 + \left[(b-b_w)h_f + \Omega_u n A_{ps}\right]c - \left[\frac{1}{2}(b-b_w)h_f^2 + \Omega_u n A_{ps} d_{ps}\right] = 0 \tag{16}$$

$$c = \frac{\sqrt{D} - (b-b_w)h_f - \Omega_u n A_{ps}}{b_w} \tag{17}$$

where

$$D = (b-b_w)h_f\left[bh_f + 2\Omega_u n A_{ps}\right] + 2\Omega_u n A_{ps} b_w d_{ps} + {\Omega_u}^2 n^2 A_{ps}^2 \tag{18}$$

and

$$I_{cr} = \frac{1}{12}(b-b_w)h_f^3 + (b-b_w)h_f\left(c-h_f\right)^2 + \frac{1}{3}b_w c^3 + \Omega_u n A_{ps}\left(d_{ps}-c\right)^2 \tag{19}$$

For rectangular sections, substitute $b = b_w$, and $\rho_{ps} = \dfrac{A_{ps}}{b d_{ps}}$ leading to:

$$D = {\Omega_u}^2 n^2 \rho_{ps}^2 + 2\Omega_u n \rho_{ps} \tag{20}$$

$$c = \left(\sqrt{D} - \Omega_u n \rho_{ps}\right) d_{ps} = k_1 d_{ps} \tag{21}$$

$$I_{cr} = \frac{1}{3} b\left(k_1 d_{ps}\right)^3 + \Omega_u n A_{ps}\left(1-k_1\right)^2 d_{ps}^2 \tag{22}$$

5.4 Verification of the proposed method

The calculated deflection of the beams are given in Table 6. The theoretical calculations are also plotted against the experimental results, which are shown from Fig. 20 to Fig. 23. As seen from Table 6, Fig. 20 and Fig. 21, all the code equations returned very good outcomes

for predicting the ultimate deflection of the beams with bonded tendons, in which the bilinear approach suggested by PCI [45] yielded the closest predictions. The maximum deflections calculated by PCI [45] for Beams C1 and C2 were 48.6 mm and 48.4 mm, which were almost equal to the experimental results of the two beams of 47.8 mm and 46.6 mm, respectively. ACI 440.4R [17] overestimated the deflections by approximately 13.4% on average compared to the experimental results while AASTHO LRFD [38] underestimated the deflection by approximately 12.3%. AASTHO LRFD [38] used factors to account for the variability in the flexural cracking strength of concrete and bonding types of prestressing tendons for computing the cracking moment. This might be the reason for the smaller deflections given by AASTHO LRFD [38]. It is noted that PCI [45] showed much smaller deflections of Beam C1 in the first elastic stage as seen in Fig. 20 since I_g was used to calculate Δ_1. Dry joints were used in Beams C1 causing the reduction in the beam's stiffness. As such, a modified moment of inertia was proposed that is presented in Eq. 13 which accounted for this stiffness reduction effect. The proposed method exhibited better predictions for the beam's deflection in the first elastic stage (Fig. 20).

In contrast, all the code equations did not predict well the deflections of Beams C3 and C4 when unbonded tendons were used. Modifications were made as presented in Section 5.3 and the predicted deflections showed a very good agreement with the experimental results as shown in Fig. 22. It, however, overestimated the ultimate deflection of Beam C4 by approximately 15% compared to the experimental results (Fig. 23). It is worth noting that substituting n by $\Omega_u n$ in Eqs. 4 and 8 will return approximately similar results as that by Eq. 22 for computation of I_{cr}.

As such, bilinear approach is recommended for calculating the deflection of the PSBs prestressed with CFRP tendons. In the first elastic stage, moment of inertia of the section, I_1, presented in Eq. 13 is used, which depends on the joint type and tendon bonding condition of

the specimen. In the second stage, I_2 is used which is taken as the moment of inertia of the cracked section, I_{cr}, which is calculated using Eq. 19 for T-section or Eq. 22 for rectangular-section.

6 Conclusion

This study investigates the use of CFRP tendons as a prestressing material on the precast segmental concrete beams. Four large-scale segmental T-shape concrete beams with either internal bonded and unbonded tendons and with dry or epoxied joints were built and tested under four-point loading. Main findings from the study are summarized as follows:

- CFRP tendons can be used to replace the steel tendons for the use in the precast segmental concrete beams to overcome the possible corrosion-induced damage. All the tested beams with CFRP tendons exhibited excellent load-carrying capacity and ductility.
- Tendon bonding condition greatly affected the flexural behavior of the segmental beams. Beams with bonded tendons showed higher strength and stiffness and larger crack mobilization while the use of unbonded tendons allowed the beams to achieve much greater ductility and less explosive failure at the ultimate stage.
- The joint type had only a slight effect on the loading capacity and ductility of the beams, but significantly affected the initial stiffness. When the joint opened, it showed an approximately linear relation with the midspan deflection of the beam under the applied loads.
- Bonded tendons almost reached its nominal tensile strength at the ultimate stage but this was not true for the cases of unbonded tendons; the unbonded tendons only achieved about 70% of the nominal tensile strength on average at the ultimate stage.
- AASTHO [26] and ACI 440.4R [17] predicted well the tendon stress, thus the load-carrying capacity at the ultimate stage of the beams with bonded tendons. However,

the accuracy significantly reduced for the cases of the beams with unbonded tendons, which requires further investigation.

- Similarly, PCI [45], AASTHO LRFD [38] and ACI 440.4R [17] predicted well the deflection capacities of the beams with bonded tendons, but the prediction accuracy largely varied for the beams with unbonded tendons.
- The proposed method for estimating the beam deflections took consideration of the stiffness reduction of the beam for dry joints and unboned tendons, and the estimated results showed very good agreement with the experimental results.

7 Acknowledgements

The authors would like to thank staff at the Civil Engineering laboratory, Curtin University, especially Mr. Mick Elliss for their technical help during the experimental program. Thanks are also expressed to Jaxier Koa and Xyrus Dangazo, final-year students for their great help in the experimental works. Finally, the first author would like to acknowledge the Curtin Strategic International Research Scholarship (CSIRS) and Centre for Infrastructural Monitoring and Protection, School of Civil and Mechanical Engineering, Curtin University for the support of his full PhD scholarship. The first author would also like to thank Hong Duc University, Thanh Hoa, Vietnam for the support during his study course.

8 Reference

[1] Hindi A, MacGregor R, Kreger ME, Breen JE. Enhancing strength and ductility of post-tensioned segmental box girder bridges. ACI Struct J 1995;92(1):33-44.

[2] Woodward R, Williams F. Collapse of YNS-Y-GWAS Bridge, Glamorgan. Proc Inst Civ Eng 1988;84(4):635-69.

[3] Wouters J, Kesner K, Poston R. Tendon corrosion in precast segmental bridges. Transp Res Rec J Transp Res Board 1999(1654):128-32.

[4] Concrete Society Technical Report. Durable post-tensioned concrete structures. TR 72, 2002.

[5] Jiang H, Cao Q, Liu A, Wang T, Qiu Y. Flexural behavior of precast concrete segmental beams with hybrid tendons and dry joints. Constr Build Mater 2016;110:1-7.

[6] Yuan A, Dai H, Sun D, Cai J. Behaviors of segmental concrete box beams with internal

tendons and external tendons under bending. Eng Struct 2013;48:623-34.

[7] Li G, Yang D, Lei Y. Combined shear and bending behavior of joints in precast concrete segmental beams with external tendons. J Bridge Eng 2013;18(10):1042-52.

[8] MacGregor RJG. Evaluation of strength and ductility of a three-span externally post-tensioned box girder bridge model: University of Texas at Austin; 1989.

[9] Aparicio AC, Ramos G, Casas JR. Testing of externally prestressed concrete beams. Eng Struct 2002;24(1):73-84.

[10] Yuan A, He Y, Dai H, Cheng L. Experimental Study of Precast Segmental Bridge Box Girders with External Unbonded and Internal Bonded Posttensioning under Monotonic Vertical Loading. J Bridge Eng 2014;20(4):04014075.

[11] Jiang H, Chen L, Ma ZJ, Feng W. Shear Behavior of Dry Joints with Castellated Keys in Precast Concrete Segmental Bridges. J Bridge Eng 2015;20(2):04014062.

[12] Shamass R, Zhou X, Alfano G. Finite-Element Analysis of Shear-Off Failure of Keyed Dry Joints in Precast Concrete Segmental Bridges. J Bridge Eng 2014;20(6):04014084.

[13] Saibabu S, Srinivas V, Sasmal S, Lakshmanan N, Iyer NR. Performance evaluation of dry and epoxy jointed segmental prestressed box girders under monotonic and cyclic loading. Constr Build Mater 2013;38:931-40.

[14] Forouzannia F, Gencturk B, Dawood M, Belarbi A. Calibration of Flexural Resistance Factors for Load and Resistance Factor Design of Concrete Bridge Girders Prestressed with Carbon Fiber–Reinforced Polymers. J Compos Constr 2016;20(2):04015050.

[15] Heo S, Shin S, Lee C. Flexural Behavior of Concrete Beams Internally Prestressed with Unbonded Carbon-Fiber-Reinforced Polymer Tendons. J Compos Constr 2013;17(2):167-75.

[16] Dolan CW, Swanson D. Development of flexural capacity of a FRP prestressed beam with vertically distributed tendons. Compos B Eng 2002;33(1):1-6.

[17] ACI 440.4R. Prestressing concrete structures with FRP tendons. Farmington Hills, USA: American Concrete Institute; 2004.

[18] Lou T, Lopes SMR, Lopes AV. A comparative study of continuous beams prestressed with bonded FRP and steel tendons. Compos Struct 2015;124:100-10.

[19] Tan KH, Tjandra RA. Strengthening of RC continuous beams by external prestressing. J Struct Eng 2007;133(2):195-204.

[20] Pisani MA. A numerical survey on the behaviour of beams pre-stressed with FRP cables. Constr Build Mater 1998;12(4):221-32.

[21] Lou T, Lopes SM, Lopes AV. Response of continuous concrete beams internally prestressed with unbonded FRP and steel tendons. Compos Struct 2016;154(2016):92-105.

[22] Mutsuyoshi H, Machida A. Behavior of Prestressed Concrete Beams Using FRP as External Cable. Spec Publ 1993;138:401-18.

[23] Grace NF, Abdel-Sayed G. Behavior of externally draped CFRP tendons in prestressed concrete bridges. PCI J 1998;43(5):88-101.

[24] Wang X, Shi J, Wu G, Yang L, Wu Z. Effectiveness of basalt FRP tendons for strengthening of RC beams through the external prestressing technique. Eng Struct 2015;101:34-44.

[25] Quayle TG. Tensile-flexural Behaviour of Carbon-fibre Reinforced Polymer (CFRP)

Prestressing Tendons Subjected to Harped Profiles: MS thesis. Univ. Waterloo; 2005.

[26] AASHTO. Guide Specifications for Design and Construction of Segmental Concrete Bridges, 2nd Ed with 2003 Interim Revis. Washington, DC: American Association of State Highway and Transportation Officials; 1999.

[27] Zhou X, Mickleborough N, Li Z. Shear strength of joints in precast concrete segmental bridges. ACI Struct J 2005;102(1):3.

[28] ACI 318-14. Building code requirements for structural concrete and commentary: American Concrete Institute. International Organization for Standardization; 2015.

[29] Dextra Group. CFRP tendons. https://wwwdextragroupcom/offices/dextra-building-products-limited.

[30] Sika Australia. Sikadur-30. https://aussikacom/.

[31] Sika Australia. SikaGrout-300PT. https://aussikacom/.

[32] Park R. Evaluation of ductility of structures and structural assemblages from laboratory testing. Bull N Z Natl Soc Earthq Eng 1989;22(3):155-66.

[33] Le TD, Pham TM, Hao H, Hao Y. Flexural behaviour of precast segmental concrete beams internally prestressed with unbonded CFRP tendons under four-point loading. Eng Struct 2018;168:371-83.

[34] Pham TM, Le TD, Hao H. Behaviour of Precast Segmental Concrete Beams Prestressed with CFRP Tendons. Proc, 9th International Conference on Fibre-Reinforced Polymer (FRP) Composites in Civil Engineering (CICE 2018) 2018:945-53.

[35] Tao X, Du G. Ultimate stress of unbonded tendons in partially prestressed concrete beams. PCI J 1985;30(6):72-91.

[36] Mattock AH, Yamazaki J, Kattula BT. Comparative study of prestressed concrete beams, with and without bond. J Proc 1971;68(2):116-25.

[37] Naaman AE, Alkhairi F. Stress at ultimate in unbonded prestressing tendons: Part 2—Proposed Methodology. ACI Struct J 1991;88(6):683-92.

[38] AASHTO LRFD. Bridge Construction Specifications, 6th Edition, U.S. Units. Washington, DC: American Association of State Highway and Transportation Officials; 2012.

[39] Harajli MH. On the stress in unbonded tendons at ultimate: Critical assessment and proposed changes. ACI Struct J 2006;103(6):803.

[40] Lee L-H, Moon J-H, Lim J-H. Proposed methodology for computing of unbonded tendon stress at flexural failure. Struct J 1999;96(6):1040-8.

[41] Roberts-Wollmann CL, Kreger ME, Rogowsky DM, Breen JE. Stresses in external tendons at ultimate. ACI Struct J 2005;102(2):206.

[42] Lou T, Xiang Y. Effects of ordinary tension reinforcement on the response of beams with unbonded tendons. Adv Struct Eng 2007;10(1):95-109.

[43] He Z, Liu Z. Stresses in External and Internal Unbonded Tendons: Unified Methodology and Design Equations. J Struct Eng 2010;136(9):1055-65.

[44] Harajili M, Kanj M. Ultimate flexural strength of concrete members prestressed with unbonded tendons. Struct J 1992;88(6):663-74.

[45] PCI. Design Handbook. Precast/Prestressed Concrete Institute (6 th), Chicago, IL 2004.

[46] Branson DE. Deformation of concrete structures: McGraw-Hill Companies; 1977.

[47] Naaman AE. Prestressed Concrete Analysis and Design. Fundamentals, USA 2004:1-1072.

9 List of figures

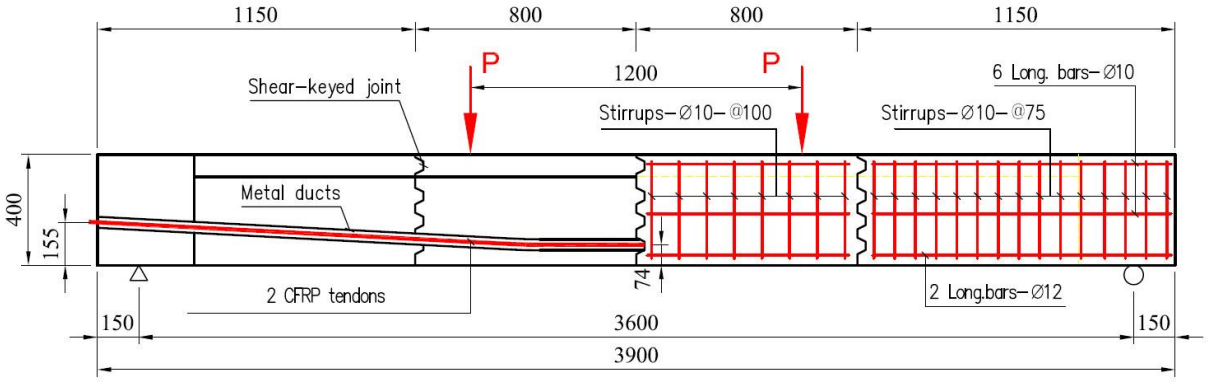

Fig. 1. Detailed dimensions of the tested beams

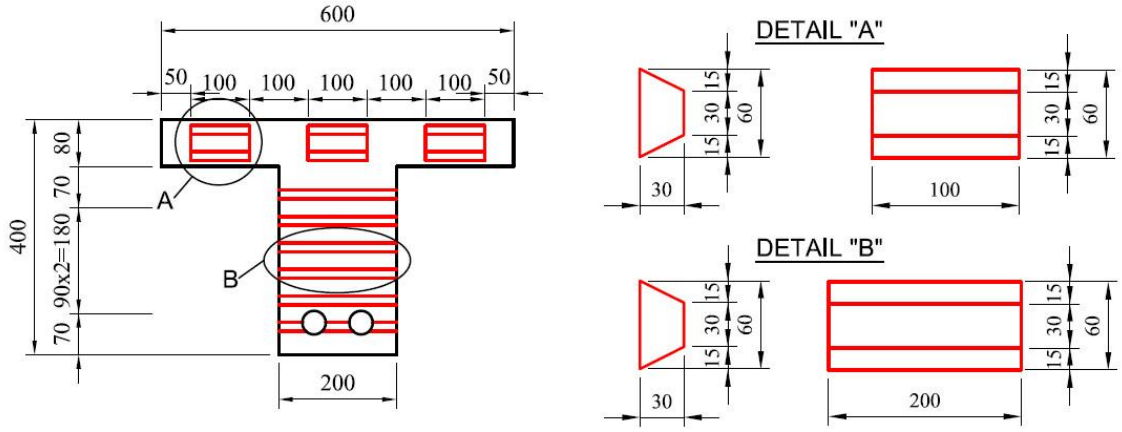

Fig. 2. Typical cross-section and multiple shear-keyed joint

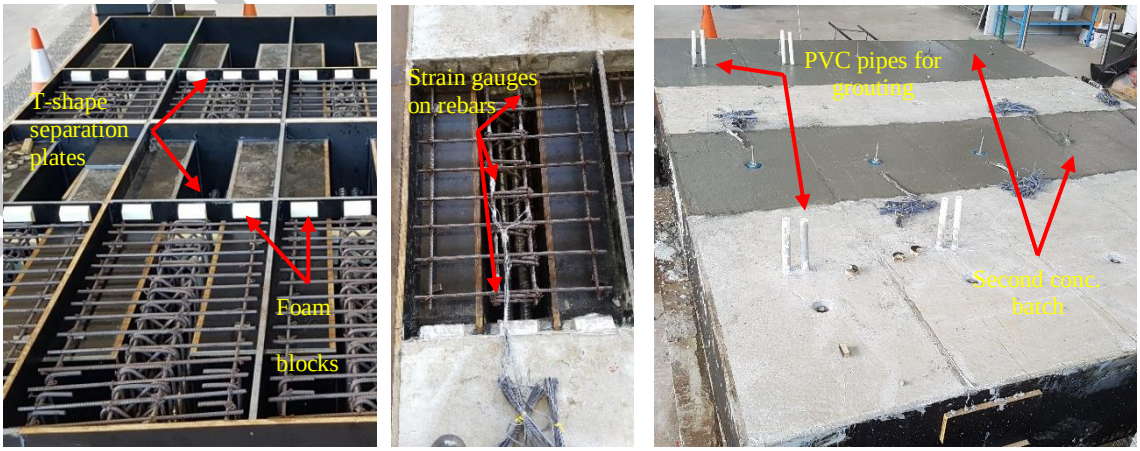

Fig. 3. Casting of the specimens

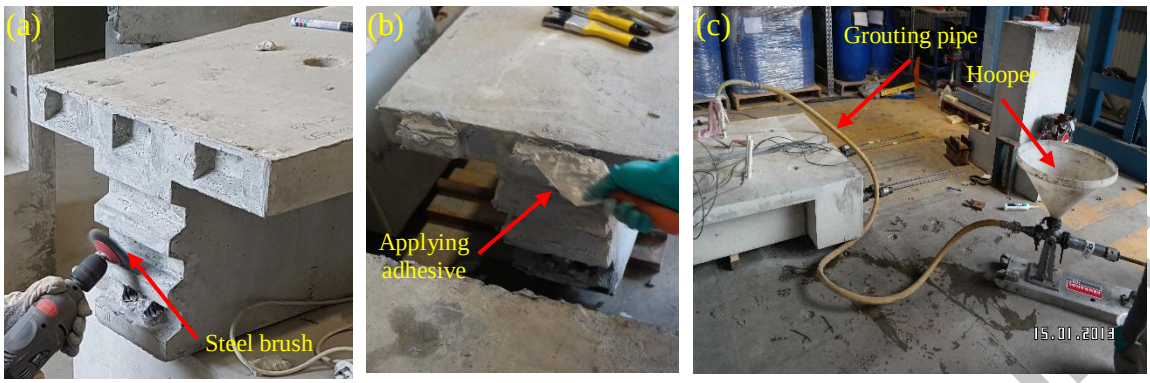

Fig. 4. Epoxy and grouting

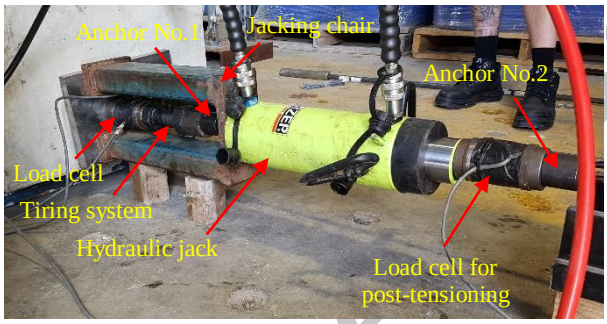

Fig. 5. Typical set up for post-tensioning

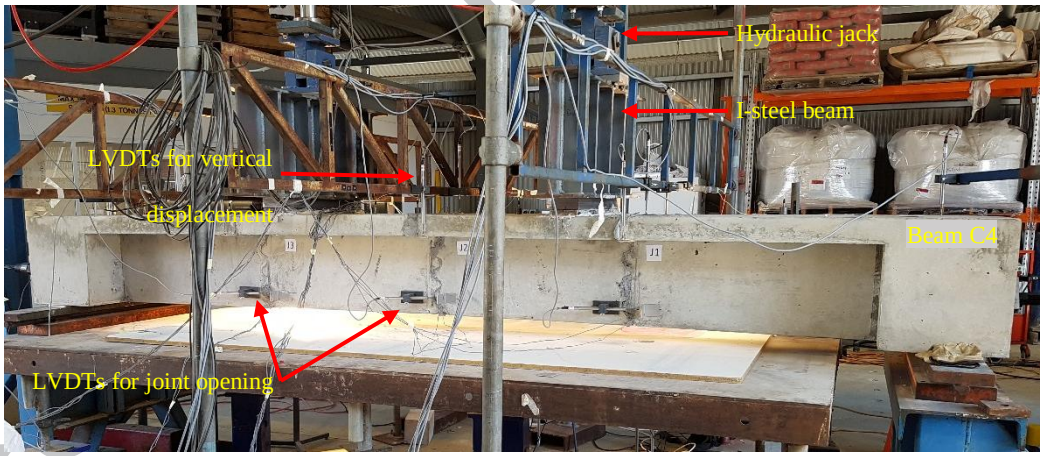

Fig. 6. Typical test set up

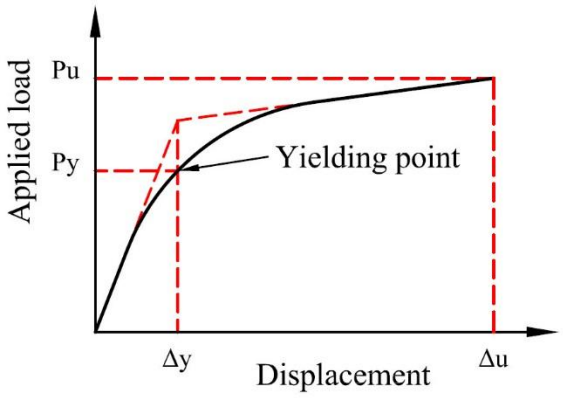

Fig. 7. Definition of yielding point

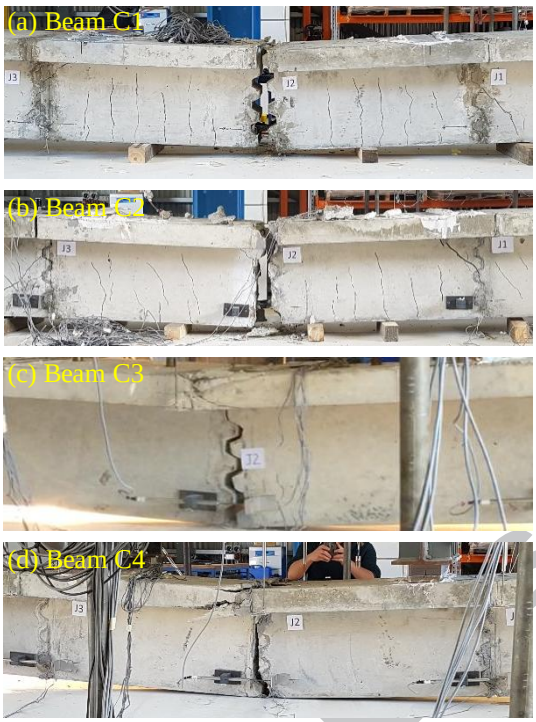

Fig. 8. Failure modes of the tested beams

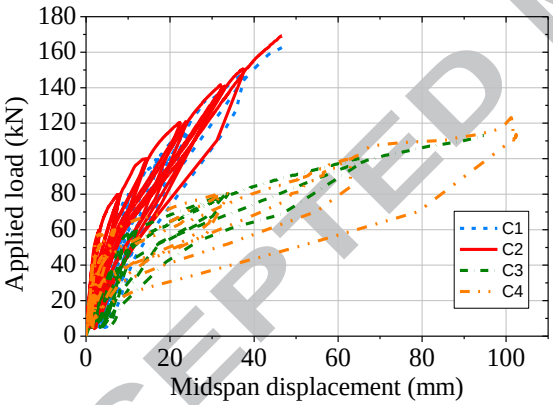

Fig. 9. Load vs deflection curves

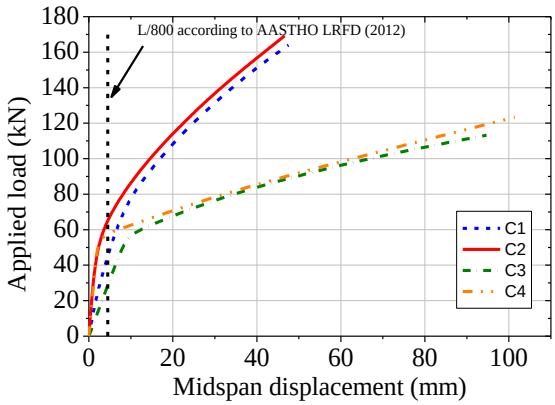

Fig. 10. Envelop curves of load vs deflection

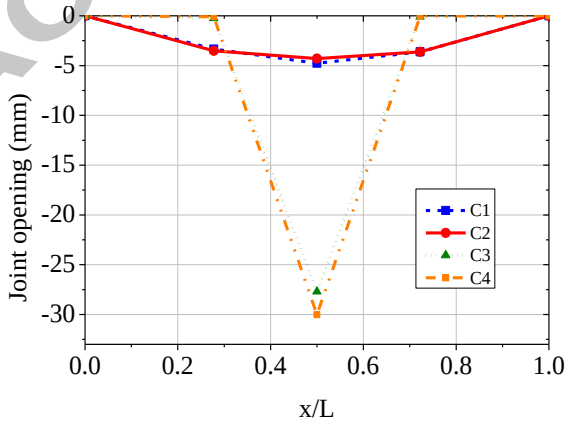

Fig. 11. Joint openings along the beam's axis

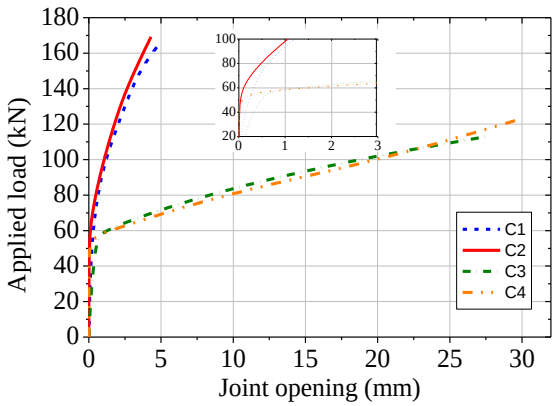

Fig. 12. Load vs opening of the middle joint

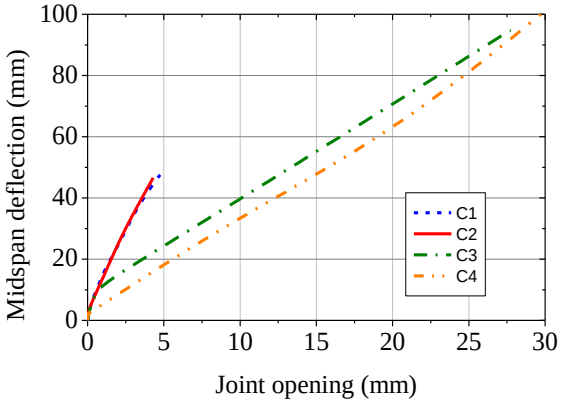

Fig. 13. Joint opening vs midspan deflection

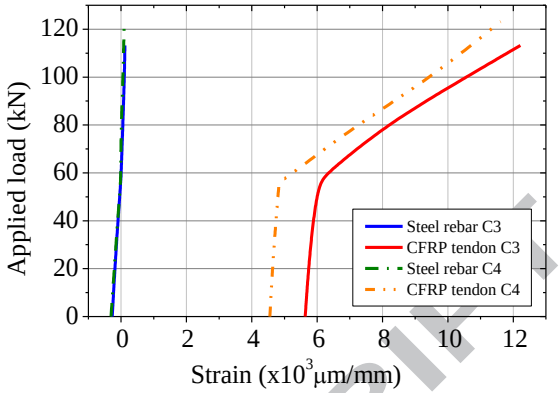

Fig. 14. Load vs strain of Beams C3 and C4

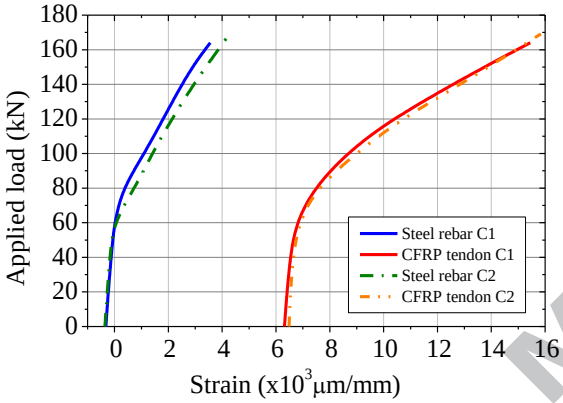

Fig. 15. Load vs strain of Beams C1 and C2

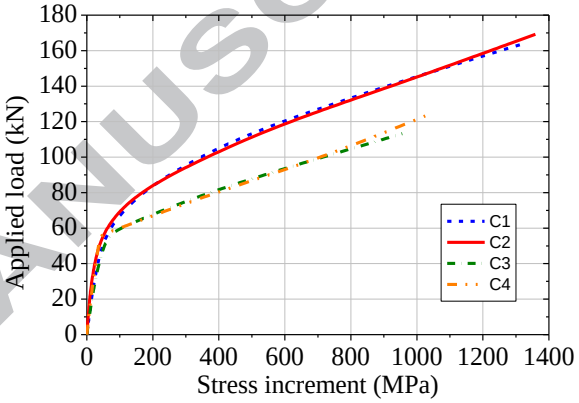

Fig. 16. Stress increment in the tendons

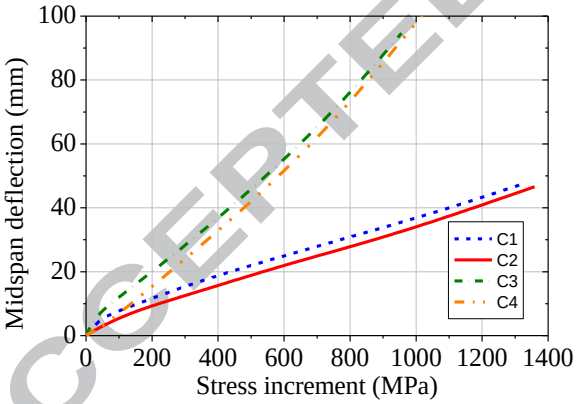

Fig. 17. Stress increment vs midspan deflection

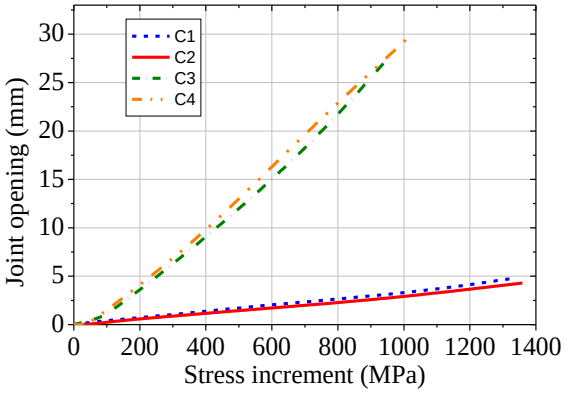

Fig. 18. Stress increment vs joint opening

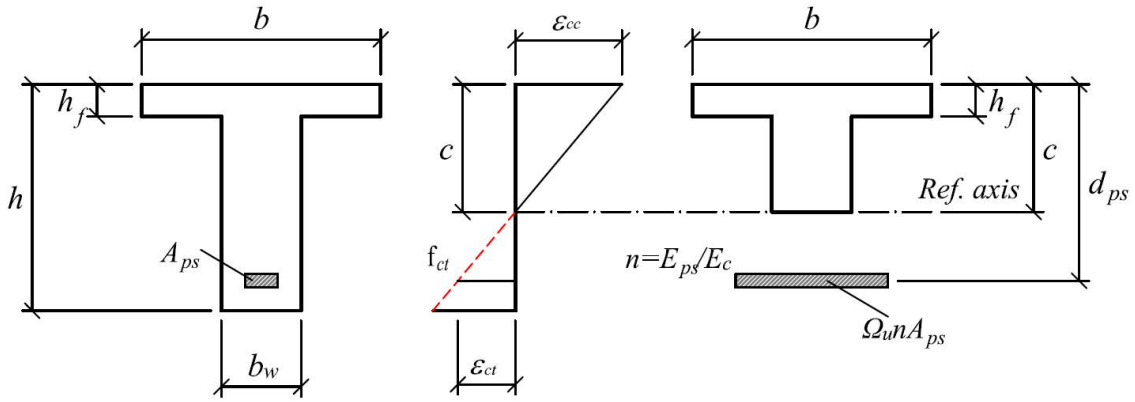

Fig. 19. Transformed concrete section

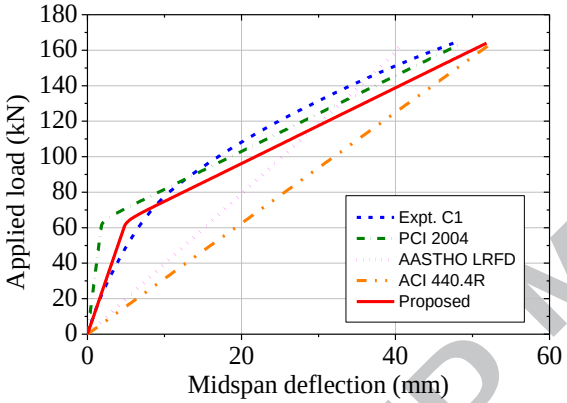

Fig. 20. Comparison of load vs deflection curves of Beam C1

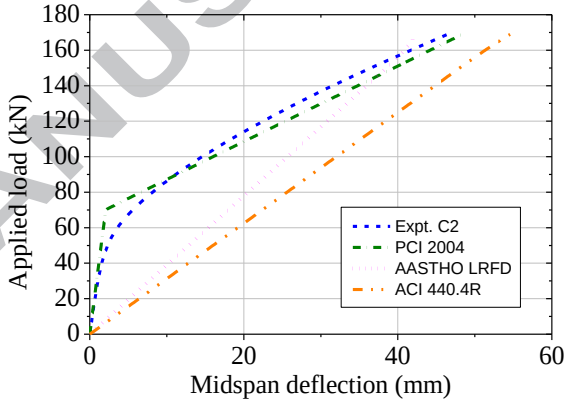

Fig. 21. Comparison of load vs deflection curves of Beam C2

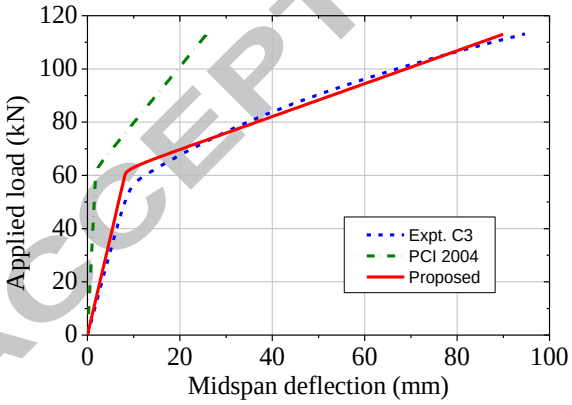

Fig. 22. Comparison of load vs deflection curves of Beam C3

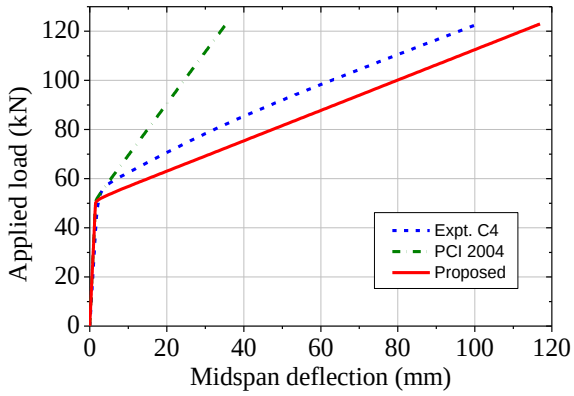

Fig. 23. Comparison of load vs deflection curves of Beam C4

10 List of Tables

Table 1
Configuration of specimens.

Beam	Bonding type	Joint type	f'_c (MPa)	f_{pe} (MPa)	f_{pe}/f_{pu}	P_{pe} (kN)
C1	Bonded	Dry	44	917	0.37	116
C2	Bonded	Epoxied	44	942	0.38	119
C3	Unbonded	Dry	44	818	0.33	104
C4	Unbonded	Epoxied	44	661	0.27	84

Table 2
Material properties.

Type	Dia. (mm)	Area (mm^2)	f_y (MPa)	f_u (MPa)	E (GPa)
Steel bar	12.0	113.0	534	587	200
Steel bar	10.0	78.5	489	538	200
CFRP tendon	12.9	126.7	N/A	2450	145

Table 3
Testing results.

Beam	Cracking			Ultimate		
	P_{cr}	$\delta_{mid,cr}$	$\Delta_{J,cr}$	P_u	$\delta_{mid,u}$	$\Delta_{J,u}$
C1	54.5*	6.9*	0.26*	164	47.8	4.73
C2	56.4	2.9	0.04	169	46.6	3.51
C3	53.4*	8.4*	0.55*	113	94.7	27.70
C4	54.1	2.3	0.07	123	101.1	30.02

(*) The values are defined in Fig. 7

Table 4
Theoretical calculations of tendon stress, f_{ps}.

Beam	$f_{expt.}$ (MPa)	f_{ps} (MPa)		f_{ps}/f_{expt}		f_{expt}/f_{pu}
		AASTHO 1999	ACI 440.4R	AASTHO 1999	ACI 440.4R	
C1	2243	2428	2450	1.08	1.09	0.91
C2	2301	2428	2450	1.05	1.06	0.94
C3	1774	1357	2094	0.76	1.18	0.72
C4	1687	1204	2006	0.71	1.19	0.69

Table 5

Theoretical calculations of applied load, P_u.

Beam	$P_{expt.}$ (kN)	P_{theo} (kN)		P_{theo}/P_{expt}	
		AASTHO 1999	ACI 440.4R	AASTHO 1999	ACI 440.4R
C1	164	162	164	0.99	1.00
C2	169	162	164	0.96	0.97
C3	113	93	141	0.82	1.25
C4	123	83	136	0.67	1.10

Table 6

Deformation calculations.

Beam	$I_g \times 10^6$ (mm^4)	Bilinear method			Effective method				Δ_{expt} (mm)
		PCI 2004			AASTHO LRFD		ACI 440.4R		
		$I_1 \times 10^6$ (mm^4)	$I_2 \times 10^6$ (mm^4)	Δ_1 (Proposed) (mm)	$I_{e1} \times 10^6$ (mm^4)	Δ_2 (mm)	$I_{e2} \times 10^6$ (mm^4)	Δ_3 (mm)	
C1	1669	625	105	48.6 (51.8)	199	40.5	166	52.5	47.8
C2	1669	1669	105	48.4 (N/A)	196	42.4	164	54.6	46.6
C3	1669	366	31	25.8 (89.9)	–	–	–	–	94.7
C4	1669	1669	31	35.4 (109.6)	–	–	–	–	101.1